Chapter 12
Beyond Wavelets

In previous chapters, we have introduced the theoretical foundation and practical applications related to the wavelet transform. The ability of wavelet transform in adaptive time-scale representation and decomposition of a signal into different subfrequency band presents an efficient signal analysis method without introducing calculation burden (Sweldens 1998). Consequently, it has become a prevailing tool for nonstationary signal processing (e.g., transient pattern identification and location). Given, however, the great variety of signals that appear in real-world applications, there remains plenty of room for continued advancement in the theory of the classical wavelet transform. For example, one of the limitations of the wavelet transform is to modify the base wavelet function to better analyze signals of finite length or duration, instead of infinite or periodic signals (Sweldens 1997). In addition, it has limitations in precisely capturing and defining the geometry of image edges. In this chapter, we introduce several new developments in signal and image processing that address these limitations and extend beyond the scope of the classical wavelet transform method (Jiang et al. 2006, 2008; Li et al. 2008; Zhou et al. 2010).

12.1 Second Generation Wavelet Transform

Second generation wavelet transform (SGWT), as an advanced mathematical tool for time-scale representation of signals, has been developed to overcome deficiencies of the classical wavelet transform. Specifically, the mechanism of constructing a base wavelet from the translation and dilation of a fixed function has been replaced by the so-called *lifting scheme* (Sweldens 1996, 1998). The resulting wavelet transform has the following properties (Uytterhoeven et al. 1997):

1. It is a generic method that is faster to calculate and easier to implement than the classical wavelet transform.
2. It can transform signals with a finite length without extension of the signal to infinite duration.

R.X. Gao and R. Yan, *Wavelets: Theory and Applications for Manufacturing*,
DOI 10.1007/978-1-4419-1545-0_12, © Springer Science+Business Media, LLC 2011

3. It can be applied to irregular signal samplings and extended for the determination of weighting functions.
4. Its inverse transform shares the same complexity as the forward transform.

12.1.1 Theoretical Basis of SGWT

The architecture of the lifting scheme can be illustrated in Fig. 12.1. The forward procedure of the lifting scheme, similar to its counterpart in the classical discrete wavelet transform, is to obtain both the approximation and detail of the original signal. It mainly incorporates three critical operational steps: (1) splitting, (2) prediction, and (3) updating. When starting the lifting scheme process, the signal $x(i)$ is first split into two subsets, the odd sample x_{odd} and the even sample x_{even}, by means of a sample sequence. For example, given a signal $x(i)$, where $i = 1, 2, 3, \ldots, 2n$ (n is a natural number), it will be split as:

$$\begin{cases} x_{\text{odd}} = \{x(2i-1)\} \\ x_{\text{even}} = \{x(2i)\} \end{cases}, \quad i = 1, 2, 3, \ldots, n \tag{12.1}$$

When the splitting procedure of the signal $x(i)$ is completed, the odd and even subsamples are obtained and the signal is subsampled by a factor of 2.

Following the splitting operation is the prediction operation, which predicts the odd data sample with the even data sample as:

$$\overline{x_{\text{odd}}} = P(x_{\text{even}}) \tag{12.2}$$

In (12.2), P is the prediction operator that is independent of the signal. The difference between the predicted result and the odd sample is considered as the detail of the original signal, d, described as:

$$d = x_{\text{odd}} - \overline{x_{\text{odd}}} = x_{\text{odd}} - P(x_{\text{even}}) \tag{12.3}$$

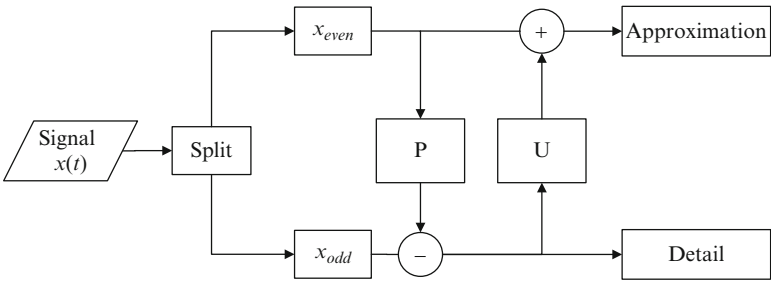

Fig. 12.1 Forward transform procedure of lifting scheme

Given the x_{even} and the detail, the approximation can be calculated with the updating operator U as:

$$a = x_{\text{even}} + U(d) \tag{12.4}$$

Similar to the prediction operation, the updating operation is also independent of the signal to be analyzed. The functions of prediction and updating operators are similar to that of a pair of $h(n)$ and $g(n)$ filters in the classical wavelet transform, and they can be derived from the scaling function $\phi(t)$ and wavelet function $\psi(t)$ by iteration algorithm (Claypoole 1999; Claypoole et al. 2003). It should be noted that the prediction and updating operators can be optimized using different algorithms, such as the Claypoole's optimization algorithm (Claypoole 1999; Claypoole et al. 2003).

Based on the forward procedure described above, the signal is decomposed into two parts: approximation and detail. This process can be iterated by taking the approximation as the input signal to continue the decomposition. Furthermore, by iterated decomposition of the detail and the approximation together, wavelet packet transform can be realized with the lifting scheme.

The decomposition is invertible, and the signal reconstruction procedure is illustrated in Fig. 12.2.

As the forward procedure realizes decomposition of the original signal, the reverse procedure realizes signal reconstruction. Similar to the forward procedure, the reverse procedure involves both the prediction operator and the updating operator. This means that the following relationship exists:

$$\begin{cases} x_{\text{odd}} = d + P(x_{\text{even}}) \\ x_{\text{even}} = a - U(d) \end{cases} \tag{12.5}$$

The signal can then be reconstructed by merging x_{even} and x_{odd}.

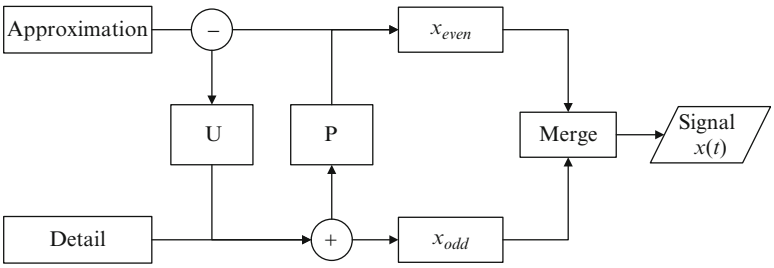

Fig. 12.2 Reverse transform procedure of lifting scheme

12.1.2 Illustration of SGWT in Signal Processing

Several examples are illustrated here on the application of the SGWT algorithm. The first example involves a signal that consists of two frequency components, sampled at 100 Hz as:

$$x(t) = \sin(2\pi \cdot 11t) + \sin(2\pi \cdot 41t) \tag{12.6}$$

The signal can be separated by one-level SGWT. Performing SGWT on this signal, where the db8 wavelet function is used as the starting point to derive the prediction and updating operators and to get the approximation part $a1$ and detailed part $d1$. The result is shown in Fig. 12.3. The accuracy of the decomposition result is evaluated through calculation of the error. Specifically, the absolute values of subtracting approximation coefficients in $a1$ and detailed coefficients in $d1$ at each sampling point from the original signal are summed up, as illustrated below:

$$\text{error} = \sum_{i=1}^{N} [x(i) - (a1(i) + d1(i))] \tag{12.7}$$

Performing the above calculation, the resulted error is only 1.26×10^{-12}, which verifies the accuracy of the decomposition.

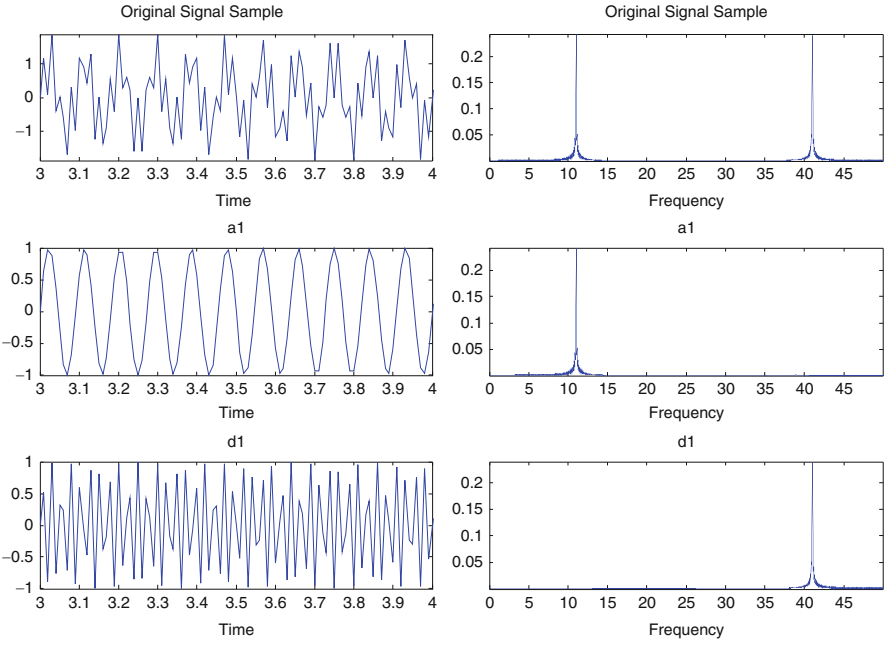

Fig. 12.3 Separation and reconstruction of two sine waves

The second example involves an intermittent linear chirp signal as expressed in (12.7):

$$x(t) = \begin{cases} \sin\left[2\pi\left(\dfrac{t+20}{3}\right)t\right] & t \in [1,4] \cup [6,9] \\ 0 & \text{else} \end{cases} \tag{12.8}$$

The signal is decomposed using the SGWT, and the results are shown in Fig. 12.4.

Adopting the same concept as that in the first example, the error of this transform is calculated as 4.09×10^{-13}, which again verifies the accuracy of the decomposition result using the SGWT.

In the area of manufacturing, surface topography has been considered as one of the factors that affect the functional performance of components. The features of a surface, such as the roughness and waviness, have direct impact on the wear rate of the component. To identify these surface features, the SGWT has been used for surface analysis (Jiang et al. 2001a, b, 2008). As an example, the bearing surface of a worn metallic femoral head is shown in Fig. 12.5a, where two different types of scratches (a regular scratch that is related to manufacturing process and a random scratch that is generated during the service time) exist (Jiang et al. 2001b). With the application of the SGWT to processing the bearing surface, the waviness feature can be clearly seen in Fig. 12.5b.

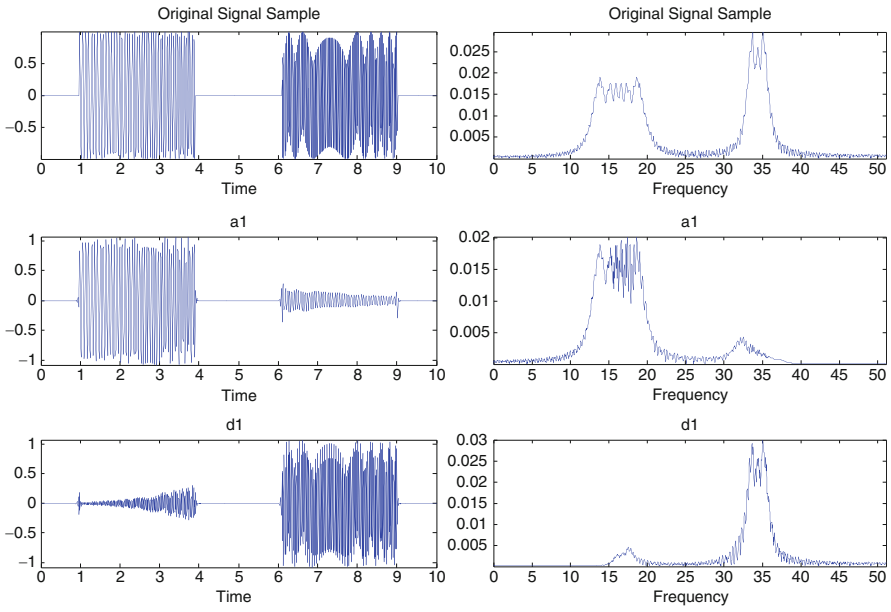

Fig. 12.4 Separation and reconstruction of intermittent linear chirp

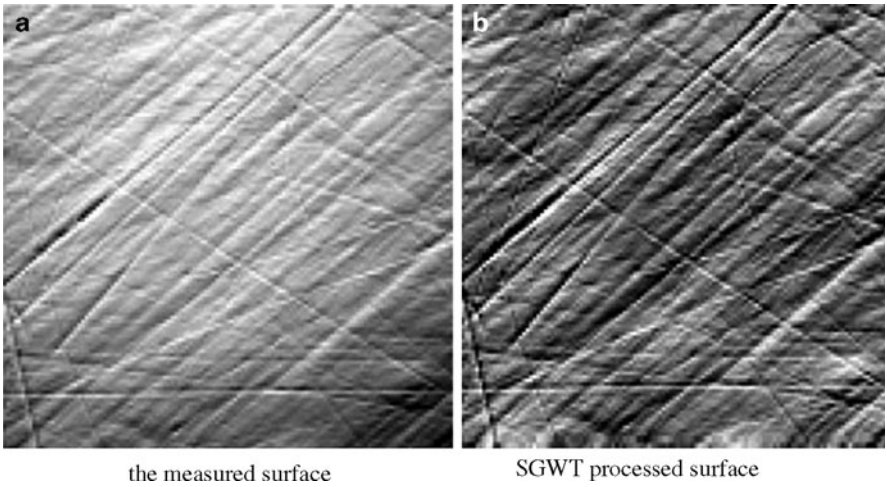

Fig. 12.5 Bearing surface of a new metallic femoral head (Jiang et al. 2001b). (**a**) The measured surface and (**b**) SGWT processed surface

12.2 Ridgelet Transform

Classical wavelet transform has been found insufficient in addressing certain problems in image processing. Prominent among the limitations is the fact that wavelets are essentially *isotropic* (i.e., its characteristics is uniform in all directions) in nature and are therefore inadequate for analyzing anisotropic features in images (Starck et al. 2006). Such constraint on the applicability of wavelets to image processing has led to research in improved methods of representation and analysis. One such method is called ridgelet analysis, which was developed by researchers at the Stanford University in 1998 (Candes 1998; Candes and Donoho 1999). The analysis is based on ridge functions that were known since the late 1970s (Logan and Shepp 1975).

12.2.1 Theoretical Basis of Ridgelet Transform

Ridgelets and the associated ridgelet analysis present a multiscale representation of mathematical functions through the superposition of *ridge* functions. The ridge functions are expressed as $r(a_1x_1 + a_2x_2 + \cdots + a_nx_n)$ (Candes and Donoho 1999). They are a set of functions with n variables, and are constant along the hyperplanes $a_1x_1 + a_2x_2 + \cdots + a_nx_n = c$. A graphical representation of the ridgelet functions is given in Fig. 12.6.

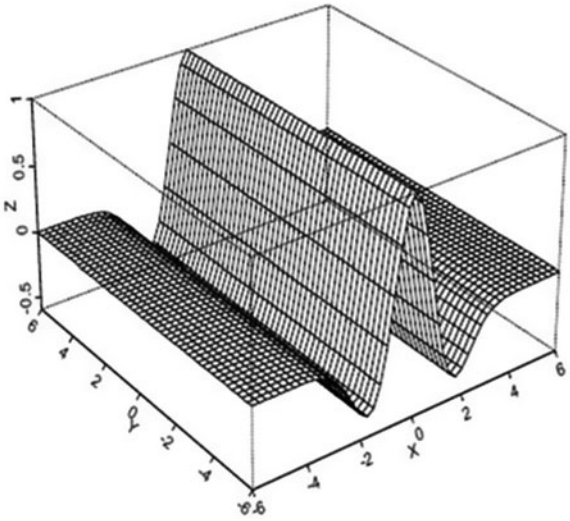

Fig. 12.6 A ridgelet with ridge functions marked by lines parallel to y-axis (Starck et al. 2003)

Furthermore, a ridge function can also be expressed as a multivariate function ($f : \mathbb{R}^n \rightarrow \mathbb{R}$) of a set of real numbers as

$$f(x_1, x_2, \ldots, x_n) = g(a_1 x_1 + \cdots + a_n x_n) = g(ax) \tag{12.9}$$

where $g : \mathbb{R} \rightarrow \mathbb{R}$ is a function of a set of real numbers, and $a = (a_1, a_2, \ldots, a_n) \in \mathbb{R}$ is a vector representing the direction. The multivariate function f with n variables can be further approximately represented by a superposition of m ($m < n$) ridge functions (Candes 1998; Candes and Donoho 1999; Starck et al. 2006) as

$$f(x_1, x_2, \ldots, x_n) \approx \sum_{i=1}^{m} c_i \sigma(a_{i1} x_1 + a_{i2} x_2 + \cdots + a_{in} x_n) \tag{12.10}$$

where c_i denotes the coefficients and m denotes the number of ridge functions.

Ridgelet transform is associated with the ridge functions, and the concept of ridgelet transform is similar to that of the Fourier transform in that it is associated with the periodic sine and cosine functions, as mathematically expressed below.

Consider a smooth, univariate function ψ, such that $\psi : \mathbb{R} \rightarrow \mathbb{R}$, with a vanishing mean, $\int \psi(t)\, \mathrm{d}t = 0$. Given this function, we can further define a bivariate function $\psi_{a,b,\theta} : \mathbb{R}^2 \rightarrow \mathbb{R}^2$ as (Candes and Donoho 1999):

$$\psi_{a,b,\theta}(x) = a^{-1/2} \psi\left(\frac{x_1 \cos\theta + x_2 \sin\theta - b}{a}\right) \tag{12.11}$$

In (12.11), $x = (x_1, x_2) \in \mathbb{R}^2$, $a>0$ is the dilation parameter, $b \in \mathbb{R}$ represents the translation parameter, and $\theta \in [0,2\pi)$ represents the direction parameter.

Equation (12.11) represents a ridgelet, whereas the dilation and translation parameters given above perform the function of scaling and translating the ridgelet, similar to the dilation (by the scaling factor s) and translation (by the time constant τ) operations in a wavelet. The function $\psi_{a,b,\theta}(x)$ is constant along the lines (i.e., ridges) $x_1 \cos\theta + x_2 \sin\theta =$ constant. Transverse to these ridges, it is a wavelet function. Accordingly, the continuous ridgelet transform of any integrable bivariate function can be expressed as (Candes 1998; Candes and Donoho 1999; Starck et al. 2006).

$$R_{\mathrm{f}}(a,b,\theta) = \int \psi_{a,b,\theta}(x) f(x)\,\mathrm{d}x \tag{12.12}$$

It is interesting to note that $\psi_{a,b,\theta}$ is defined on the $\mathbb{R}^2$ space and the associated transform is therefore 2D. The inverse of (12.12) used in reconstruction is given as (Candes and Donoho 1999)

$$f(x) = \int_0^{2\pi} \int_{-\infty}^{\infty} \int_0^{\infty} \frac{4\pi}{a^3} R_{\mathrm{f}}(a,b,\theta)\, \psi_{a,b,\theta}(x)\,\mathrm{d}a\,\mathrm{d}b\,\mathrm{d}\theta \tag{12.13}$$

12.2.2 Application of the Ridgelet Transform

The 2D nature of the ridgelet transform makes it very well suited for analyzing and processing images. Prominent ridgelet applications include denoising, edge detection, and classification of tissues from images of internal human organs. As an example, Fig. 12.7 shows two images of a supernova before and after denoising using ridgelets, respectively (Starck et al. 2003).

It can be seen that the original x-ray image (the left side of Fig. 12.7) is blurred by the noise, while the image becomes clear after the noise has been filtered out using the ridgelet transform (the right side of Fig. 12.7).

Another example of the application of the ridgelet transform is to characterize surface topography (Ma et al. 2005). This is an important issue, as it has impacts on the mechanical and physical properties of the system. Figure 12.8 shows the results of extracting deep scratches from a honed surface, which were seen in an automotive engine cylinder (Ma et al. 2005). Their distribution of such scratches on the surface and their amplitudes directly affect the gas or air flow and pressure balance in an engine. In Fig. 12.8b, deep scratches are reconstructed by means of a ridgelet transform.

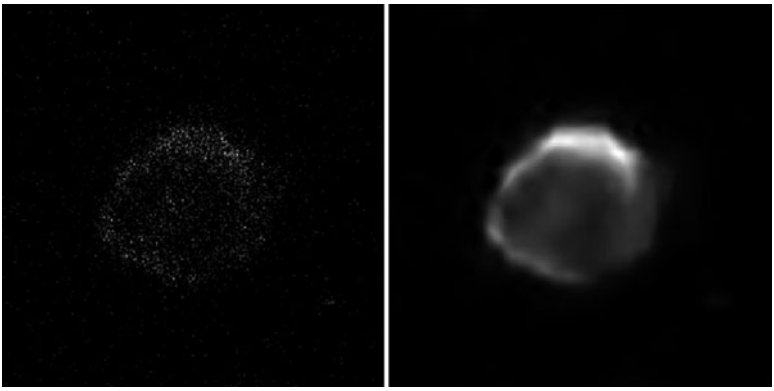

Fig. 12.7 Image denoising using the ridgelet transform. Reproduced from Starck et al. (2003)

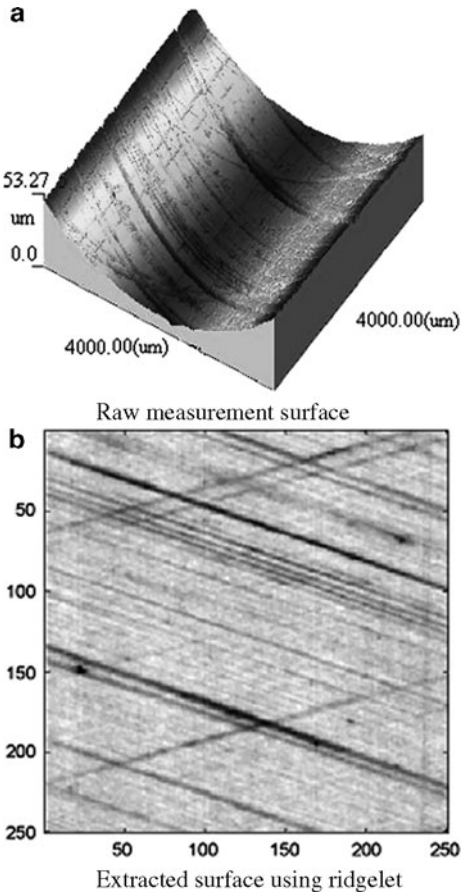

Fig. 12.8 Extraction of linear scratches from a honed surface of the automotive engine cylinder (Ma et al. 2005). (**a**) Raw measurement surface and (**b**) extracted surface using ridgelet

12.3 Curvelet Transform

Ridgelet transform is a relatively new system of representation and analysis, which has been shown to be effective in resolving edges (Candes and Donoho 1999; Do and Vetterli 2003; Dettori and Semler 2007). However, ridgelets are limited to resolving only straight edges; curved edges cannot be represented with as few coefficients as required for a straight edge (Do and Vetterli 2003; Starck et al. 2003). The inadequacy of wavelets and ridgelets in resolving edges has been the primary driving force behind the search for better representation and analysis. Curvelet analysis, introduced in the year 2000 (Candes and Donoho 2000), holds potential in addressing the shortcomings of wavelets and ridgelets. A brief introduction to the fundamentals of curvelets is given in this section.

12.3.1 Curvelet Transform

The curvelet transform is defined as the inner product of the function f to be analyzed and a family of curvelets $\gamma_{ab\theta}$ (Candes and Donoho 2000, 2005a, b):

$$\Gamma_{\mathrm{f}}(a,b,\theta) = \langle f, \gamma_{ab\theta} \rangle \tag{12.14}$$

where $a>0$ is the scale parameter, b is the translation parameter, and $\theta \in [0, 2\pi)$ is the orientation parameter. The symbol Γ_{f} represents the curvelet transform. The family of curvelets is explained by starting with two smooth, nonnegative, real valued windowing functions called the *radial* window $W(r)$ and the *angular* window $V(t)$, respectively (Candes and Donoho 2005a, b). The two windowing functions are subject to the following two admission conditions:

$$\int_0^\infty \frac{1}{a} W(ar)^2 \, \mathrm{d}a = 1, \quad \forall\, r>0 \tag{12.15}$$

$$\int_{-1}^{1} V(t)^2 \, \mathrm{d}t = 1 \tag{12.16}$$

In (12.5), $r \in (1/2, 2)$ is the radial coordinate and in (12.6) $t \in [-1, 1]$ denotes the time variable. According to the definition in (12.14), at a given scale a, a family of curvelets can be generated by translation and rotation of a basic element γ_{a00} as shown in (12.17) (Candes and Donoho 2005a, b):

$$\gamma_{ab\theta} = \gamma_{a00}(R_\theta(x-b)) \tag{12.17}$$

where R_θ is a 2×2 rotation matrix that is related to planar rotation by an angle θ.

The basic element itself is expressed mathematically as:

$$\gamma_{a00}(r,\omega) = W(ar)\, V\left(\frac{\omega}{\sqrt{a}}\right) a^{3/4} \tag{12.18}$$

where r and ω are polar coordinates defined in the frequency domain.

Generally, the discrete curvelet transform is often used to process the function f, which also starts with two window functions: the *radial* window $W(r)$ and the *angular* window $V(t)$ (Candes et al. 2006). The transform is subject to the conditions expressed in (12.19)–(12.21) as:

$$\sum_{j=-\infty}^{\infty} W(2^j r)^2 = 1 \tag{12.19}$$

$$\sum_{l=-\infty}^{\infty} V(t-l)^2 = 1 \tag{12.20}$$

$$U_j(r,\theta) = 2^{-3j/4} W(2^{-j} r) V\left(\frac{2^{\lfloor j/2 \rfloor}\theta}{2\pi}\right) \tag{12.21}$$

In (12.21), the window function U_j is derived from the radial window $W(r)$ and the angular window $V(t)$ and expressed in the Fourier domain. The symbols $r \in (3/4, 3/2)$ and θ denote polar coordinates, and $t \in (-1/2, 1/2)$ is the time variable.

Based on these notations, a family of curvelets at a fixed scale of 2^j is defined as:

$$\varphi_{j,l,k}(x) = \varphi_j(R_{\theta_l}(x - x_k^{(j,l)})) \tag{12.22}$$

where $x_k^{(j,l)} = R_{\theta_l}^{-1}(k_1 2^{-j},\ k_2 2^{-j/2})$ represents the position information, and $R_\theta = \begin{pmatrix} \cos\theta & \sin\theta \\ -\sin\theta & \cos\theta \end{pmatrix}$ represents the rotation information in terms of θ radians, respectively.

Accordingly, the inner product between a curvelet $\varphi_{j,l,k}$ and a function f results in the curvelet coefficients as:

$$c(j,l,k) = \langle f, \varphi_{j,l,k} \rangle = \int_{\mathbb{R}^2} f(x)\ \varphi_{j,l,k}(x)\, \mathrm{d}x \tag{12.23}$$

where $c(j,l,k)$ are the curvelet coefficients.

The physical interpretation of (12.23) in the Fourier domain at a scale of 2^j can be illustrated in Fig. 12.9. The concentric circles represent the family of curvelets $\varphi_{j,l,k}(x)$ and the shaded portion represents one curvelet from this family.

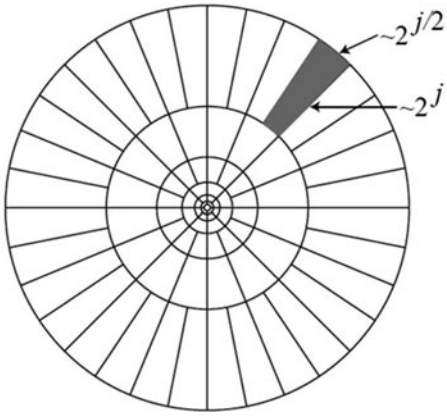

Fig. 12.9 A family of curvelets in polar coordinates, with the shaded area representing support for a single curvelet (Candes et al. 2006)

While the curvelets described above are expressed in the polar coordinates, Cartesian coordinates are desirable to implement the curvelet transform (Donoho and Duncan 2000; Candes et al. 2006). Consequently, the window functions expressed in (12.19)–(12.21) are expressed in the Cartesian coordinates as

$$W_j(\omega) = \sqrt{\Phi^2_{j+1}(\omega) - \Phi^2_j(\omega)}, \quad j>0 \tag{12.24}$$

$$V_j(\omega) = V\left(\frac{2^{\lfloor j/2 \rfloor}\omega_2}{\omega_1}\right) \tag{12.25}$$

$$U_j(\omega) = W_j(\omega)\, V_j(\omega) \tag{12.26}$$

where $\Phi(\omega_1, \omega_2) = \phi(2^{-j}\omega_1)\phi(2^{-j}\omega_2), 2^j \le \omega_1 \le 2^{j+1}, -2^{-j/2} \le (\omega_2/\omega_1) \le 2^{-j/2}$, and $0 \le \phi \le 1$, $\phi = \begin{cases} 1, [-1/2, 1/2] \\ 0, [-2, 2] \end{cases}$.

Currently, there are two prevalent methods of calculating the curvelet coefficients. The first method, called the digital curvelet transform via unequispaced fast Fourier transform (Candes et al. 2006), involves the following four steps:

1. Calculate the 2D FT of the function of interest $(f[t_1, t_2])$, to obtain its Fourier samples, $\hat{f}[n_1, n_2]$.
2. Resample $\hat{f}[n_1, n_2]$ for each scale/angle pair (j, l) to obtain sampled values $\hat{f}[n_1, n_2 - n_1 \tan\theta_l]$.
3. Multiply the resampled $\hat{f}$ with the window function U_j, to obtain $\tilde{\hat{f}}_{j,l}[n_1, n_2] = \hat{f}[n_1, n_2 - n_1 \tan\theta_l]\ U_j[n_1, n_2]$, where $\tan\theta_l = l\,2^{-\lfloor j/2 \rfloor}$.
4. Calculate the inverse of the 2D FT of every $\tilde{\hat{f}}_{j,l}$ to obtain the discrete curvelet coefficients, $c(j, l, k)$.

The second method is called digital curvelet transform via wrapping (Candes et al. 2006), and involves the following computational steps:

1. Calculation of 2D FT of the function of interest $(f[t_1, t_2])$, to obtain its Fourier samples, $\hat{f}[n_1, n_2]$.
2. Calculation of the product $U_{j,l}[n_1, n_2]\, \hat{f}[n_1, n_2]$.
3. Wrapping the product $U_{j,l}[n_1, n_2]\, \hat{f}[n_1, n_2]$ around the origin to obtain $\tilde{f}_{j,l}[n_1, n_2] = W(U_{j,l}\, \hat{f})[n_1, n_2]$.
4. Calculation of inverse 2D FFT of every $\tilde{f}_{j,l}$ to obtain discrete curvelet coefficients, $c(j, l, k)$.

12.3.2 Application of the Curvelet Transform

Because of its multiscale nature, most of the curvelet applications are related to image processing. Specifically, the curvelet transform has been applied to image compression, contrast enhancement, feature extraction from noisy images, pattern detection, noise filtration, edge detection, etc. As an example, a denoising operation on a test image "Lena" is shown in Fig. 12.10. This image, which is 512 × 512 pixels in size (Fig. 12.10a), was contaminated with random noise (peak signal-to-noise ratio, PSNR: 22.1), as shown in Fig. 12.10b. Curvelet transform is then applied for image denoising via thresholding of its curvelet coefficients. The result is a filtered image as seen in Fig. 12.10c, which has an improved PSNR value of 31.1.

In manufacturing, the curvelet has been used for surface characterization. Fig 12.11a shows a surface of a worn metallic femoral head. When additive white noise is added into it, the surface has a signal-to-noise ratio (SNR) of 56.43 dB. When the wavelet transform is used to remove the noise, the SNR of the surface has increased to 58.72 dB. Finally, the performance of the denoising operation was further improved when the curvelet transform is applied to process the surface, where the SNR has increased to 61.62 dB.

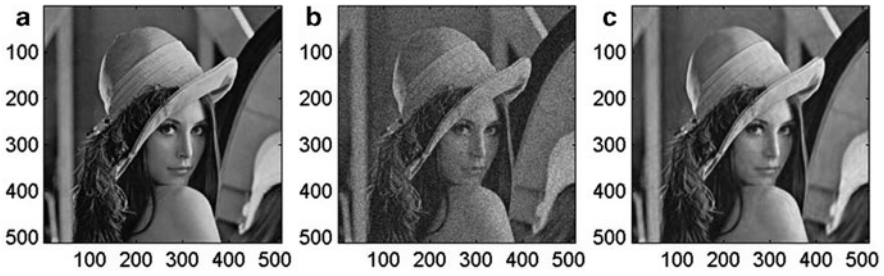

12.10 (**a**) Original image, (**b**) image contaminated with noise, and (**c**) image after denoising

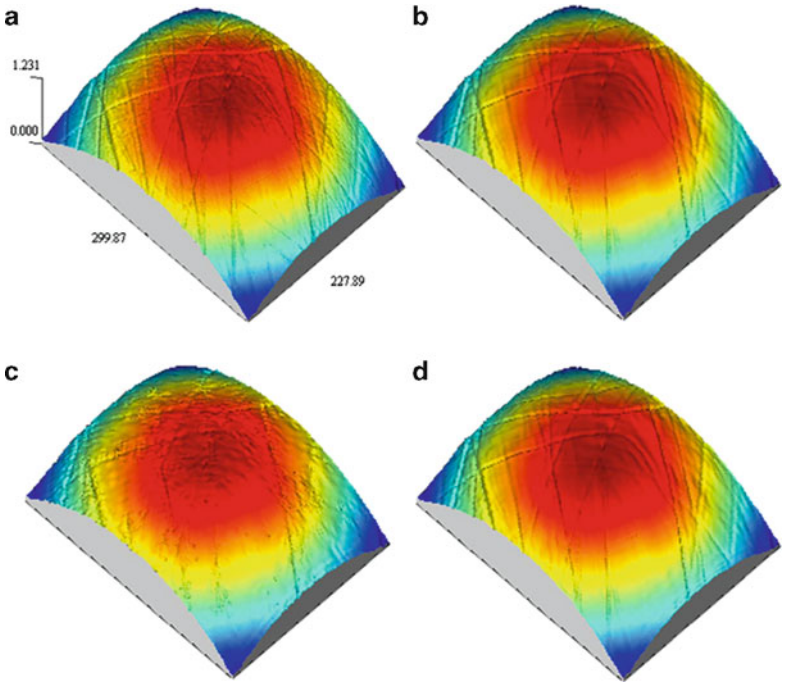

Fig. 12.11 Denoising of a microscalar surface (Ma 2007). (**a**) Original surface (scale unit: μm), (**b**) noisy surface (signal-to-noise ratio, SNR = 56.43 dB), (**c**) denoised surface using wavelet (SNR = 58.72 dB), and (**d**) denoised surface using curvelet (SNR = 61.62 dB)

12.4 Summary

This chapter briefly presents development in signal processing that goes beyond the classical wavelet transform. The SGWT based on the lifting scheme is first introduced to allow for the design of the base wavelet functions to better fit the signal to be analyzed. The ridgelet and curvelet transforms are then introduced from the point of view of overcoming the limitations in detecting edges (straight and curved) of images when applying the classical wavelet transform. These techniques, together with further advancement reported in the literature, such as multiwavelet transform (Cotronei et al. 1998), dual-tree wavelet transform (Selesnick et al. 2005), and contourlet transform (Do and Vetterli 2005), promise to continually push the envelope of signal and image processing to better serve the needs for a wide range of engineering problems.

12.5 References

Candes EJ (1998) Ridgelets: theory and applications. Ph.D. Dissertation, Stanford University
Candes EJ, Donoho DL (1999) Ridgelets: a key to higher-dimensional intermittency. Philos Trans R Soc Math, Phys Eng Sci 357:2495–2509
Candes EJ, Donoho DL (2000) Curvelets – a surprisingly effective nonadaptive representation for objects with edges. In: Rabut C, Cohen A, Schumaker LL (eds) Curves and surfaces. Vanderbilt University Press, Nashville, TN
Candes EJ, Donoho DL (2005a) Continuous curvelet transform: 1. resolution of the wavefront set. Appl Comput Harmon Anal 19:162–197
Candes EJ, Donoho DL (2005b) Continuous curvelet transform: 2. discretization and frames. Appl Comput Harmon Anal 19:198–222
Candes EJ, Demanet L, Donoho DL, Ying L (2006) Fast discrete curvelet transforms. SIAM Multiscale Model Simul 5:861–899
Claypoole R (1999) Adaptive wavelet transforms via lifting. Thesis: computer engineering, Rice University
Claypoole R, Davis G, Sweldens W (2003) Nonlinear wavelet transform for image coding via lifting. IEEE Trans Image Process 12(12):1449–1459
Cotronei M, Montefusco LB, Puccio L (1998) Multiwavelet analysis and signal processing. IEEE Trans Circuits Syst II Analog Digital Signal Process 45(8): 970–987
Dettori L, Semler L (2007) A comparison of wavelet, ridgelet and curvelet based texture classification algorithms in computed tomography. Comput Biol Med 37:486–498
Do MN, Vetterli M (2003) The finite ridgelet transform for image representation. IEEE Trans Image Process 12:16–28
Do MN, Vetterli M (2005) The contourlet transform: an efficient directional multiresolution image representation. IEEE Trans Image Process 14(12):2091–2106
Donoho DL, Duncan MR (2000) Digital curvelet transform: strategy, implementation and experiments. Proc SPIE 4056:12–29
Jiang HK, Wang ZS, He ZJ (2006) Wavelet design for extracting weak fault feature based on lifting scheme. Front Mech Eng China 1(2):199–203
Jiang X, Blunt L, Stout KJ (2001a) Application of the lifting wavelet to rough surfaces. J Int Soc Precision Eng Nanotechnol 25:83–89
Jiang X, Blunt L, Stout KJ (2001b) Lifting wavelet for three-dimensional surface analysis. Int J Mach Tools Manuf 41:2163–2169
Jiang X, Scott P, Whitehouse D (2008) Wavelets and their application in surface metrology. CIRP Ann Manuf Technol 57:555–558
Li Z, He ZJ, Zi YY, Jiang HK (2008) Rotating machinery fault diagnosis using signal-adapted lifting scheme. Mech Syst Signal Process 22(3):542–556
Logan BF, Shepp LA (1975) Optimal reconstruction of a function from its projections. Duke Math J 42:645–659
Ma J, Jiang X, Scott P (2005) Complex ridgelets for shift invariant characterization of surface topography with line singularities. Phys Lett A 344:423–431
Ma J (2007) Curvelets for surface characterization. Appl Phys Lett 90: 054109-1-3
Selesnick IW, Baraniuk RG, Kingsbury NG (2005) The dual-tree complex wavelet transform. IEEE Signal Process Mag 22(6): 123–151
Starck JL, Donoho DL, Candes EJ (2003) Astronomical image representation by the curvelet transform. Astron Astrophys 398:785–800
Starck JL, Moudden Y, Abrial P, Nguyen M (2006) Wavelets, ridgelets and curvelets on the sphere. Astron Astrophys 446:1191–1204
Sweldens W (1996) The lifting scheme: a custom-design construction of biorthogonal wavelets. Appl Comput Harmon Anal 3:186–200

Sweldens W (1997) Second generation wavelets: theory and application. http://www.ima.umn.edu/industrial/97_98/sweldens/fourth.html. Accessed 30 June 2009

Sweldens W (1998) The lifting scheme: a construction of second generation wavelets. SIAM J Math Anal 29(2):511–546

Uytterhoeven G, Dirk R, Adhemar B (1997) Wavelet transforms using the lifting scheme. Department of Computer Science, Katholieke Universiteit Leuven, Belgium

Zhou R, Bao W, Li N, Huang X, Yu DR (2010) Mechanical equipment fault diagnosis based on redundant second generation wavelet packet transform. Digit Signal Process 20(1):276–288